

# A negative permeability material at red light

Hsiao-Kuan Yuan, Uday K. Chettiar, Wenshan Cai, Alexander V. Kildishev, Alexandra Boltasseva\*, Vladimir P. Drachev, and Vladimir M. Shalaev

*Birek Nanotechnology Center, Purdue University, West Lafayette, IN 47907, USA*

*\* on leave from DTU, Research Center COM and Nanophotonics, DK-2800 Kgs. Lyngby, Denmark  
[kildishev@purdue.edu](mailto:kildishev@purdue.edu)*

**Abstract:** A negative permeability in a periodic array of pairs of thin silver strips is demonstrated experimentally for two distinct samples. The effect of the strip surface roughness on negative permeability is evaluated. The first sample, Sample A, is fabricated of thinner strips with a root mean square roughness of 7 nm, while Sample B is made of thicker strips with 3-nm roughness. The real part of permeability,  $\mu'$ , is  $-1$  at a wavelength of 770 nm in Sample A and  $-1.7$  at 725 nm in Sample B. Relative to prototypes simulated with ideal strips, larger strip roughness acts to decrease  $|\mu'|$  by a factor of 7.8 in Sample A versus a factor of 2.4 decrease for Sample B.

©2007 Optical Society of America

**OCIS codes:** (160.4670) Optical materials, metamaterials, negative refraction, left-handed materials; (260.5740) Physical Optics, resonance; (310.6860) Thin films, optical properties.

---

## References and links

1. D. R. Smith, S. Schultz, P. Markoš, and C. M. Soukoulis, "Determination of effective permittivity and permeability of metamaterials from reflection and transmission coefficients," *Phys. Rev. B* **65**, 195104 (2002).
2. A. V. Kildishev, W. Cai, U. K. Chettiar, H.-K. Yuan, A. K. Sarychev, V. P. Drachev, and V. M. Shalaev, "Negative refractive index in optics of metal-dielectric composites," *J. Opt. Soc. Am. B* **23**, 423-433 (2006).
3. U. K. Chettiar, A. V. Kildishev, T. A. Klar, and V. M. Shalaev, "Negative index metamaterial combining magnetic resonators with metal films," *Opt. Express* **14**, 7872-7877 (2006).
4. G. Shvets and Y. A. Urzhumov, "Negative index meta-materials based on two-dimensional metallic structures," *J. Opt. A* **8**, S122 (2006).
5. V. A. Podolskiy, A. K. Sarychev, and V. M. Shalaev, "Plasmon modes in metal nanowires and left-handed materials," *J. Nonlinear Opt. Phys. Mater.* **11**, 65-74 (2002).
6. S. Zhang, W. Fan, K. J. Malloy, S. R. J. Brueck, N. C. Panoiu, and R. M. Osgood, "Demonstration of metal-dielectric negative-index metamaterials with improved performance at optical frequencies," *J. Opt. Soc. Am. B* **23**, 434-438 (2006).
7. J. Zhou, L. Zhang, G. Tuttle, T. Koschny, and C. M. Soukoulis, "Negative index materials using simple short wire pairs," *Phys. Rev. B* **73**, 041101(R) (2006).
8. T. J. Yen, W. J. Padilla, N. Fang, D. C. Vier, D. R. Smith, J. B. Pendry, D. N. Basov, and X. Zhang, "Terahertz magnetic response from artificial materials," *Science* **303**, 1494-1496 (2004).
9. S. Linden, C. Enkrich, M. Wegener, J. Zhou, T. Koschny, and C. M. Soukoulis, "Magnetic response of metamaterials at 100 Terahertz," *Science* **306**, 1351-1353 (2004).
10. S. Zhang, W. Fan, B. K. Minhas, A. Frauenglass, K. J. Malloy, and S. R. J. Brueck, "Midinfrared resonant magnetic nanostructures exhibiting a negative permeability," *Phys. Rev. Lett.* **94**, 037402 (2005).
11. C. Enkrich, M. Wegener, S. Linden, S. Burger, L. Zschiedrich, F. Schmidt, J. F. Zhou, Th. Koschny, and C. M. Soukoulis, "Magnetic metamaterials at telecommunication and Visible frequencies," *Phys. Rev. Lett.* **95**, 203901 (2005).
12. A. N. Grigorenko, "Negative refractive index in artificial metamaterials," *Opt. Lett.* **31**, 2483-2485 (2006).
13. A. V. Kildishev, V. P. Drachev, U. K. Chettiar, D. Werner, D.-H. Kwon, and V. M. Shalaev, "Comment on "Negative Refractive Index in Artificial Metamaterials," accepted for publication in *Opt. Lett.*
14. A. V. Kildishev and U. K. Chettiar, "Cascading optical negative index metamaterials," accepted for publication in the *Journal of Applied Computational Electromagnetics Society*.
15. P. B. Johnson and R. W. Christy, "Optical constants of the noble metals," *Phys. Rev. B* **6**, 4370-4379 (1972).
16. G. Dolling, M. Wegener, C. M. Soukoulis, and S. Linden, "Negative-index metamaterial at 780 nm wavelength," *Opt. Lett.* **32**, 53-55 (2007).

A thin film of a nanostructured metamaterial with physical thickness  $\delta$  can be characterized through its spectra to have an effective refractive index  $n = n' + i n''$  and an effective impedance  $\eta = \eta' + i \eta''$ . To obtain these parameters, the complex values of the transmitted and reflected fields should be available either from optical experiments or simulations [1,2]. In addition, along with its effective  $n$  and  $\eta$ , the layer can be characterized by its effective permittivity  $\varepsilon = \varepsilon' + i \varepsilon''$  and permeability  $\mu = \mu' + i \mu''$ , defined as  $\varepsilon = n/\eta$ , and  $\mu = n\eta$ . The values of  $n$  and  $\eta$  (or  $\varepsilon$  and  $\mu$ ) of the equivalent homogenized layer of thickness  $\delta$  are chosen to reproduce the complex values of far-field reflectance and transmittance due to a given film.

Optical negative index metamaterials (NIMs), also known as left-handed materials, are artificially engineered metal-dielectric composites that exhibit  $n' < 0$  within a certain range of wavelengths. In addition, a magnetic resonant behavior should be observed in NIMs at this range. The magnetic resonance in any optical NIM is always required to make the real part of the effective refractive index negative, either through the strong (sufficient) condition  $\mu' < 0$  and  $\varepsilon' < 0$ , or through a more general necessary condition  $\varepsilon'\mu'' + \mu'\varepsilon'' < 0$ , which is valid for a passive medium. The general condition strictly implies that there is no negative refraction effect in a passive metamaterial with  $\mu = 1 + 0i$ . Nonetheless, the effect is also achievable for  $\mu' > 0$  provided that only  $\varepsilon' < 0$  in  $\varepsilon'\mu'' + \mu'\varepsilon''$ , and  $|\varepsilon'\mu| > |\mu'\varepsilon|$ . In the latter case, substantial 'magnetic' losses are necessary along with a dominant metal content in the structure. We note that a ratio of  $|n'/n''|$  is often taken as a figure of merit (FOM) for NIM performance, since low-loss NIMs are desired. The FOM can be written as  $|n'/n''| = (|\varepsilon'\mu| + \mu'\varepsilon)/(\varepsilon''|\mu| + \mu''|\varepsilon|)$ , indicating that a 'double-negative' NIM ( $\mu' < 0$ ,  $\varepsilon' < 0$ ) will have a much better FOM than a NIM layer with  $\mu' > 0$ . Therefore, metal-dielectric composites with a negative effective permeability are essential for further development of low-loss optical NIMs.

Recent computational results [3,4] have demonstrated that pairs of thin silver strips separated by a dielectric spacer could offer an easy way of achieving negative magnetism by coupling near-field modes. This approach generalizes the original idea of a diamagnetic response (and negative  $n$ ) in pairs of rods [5]. It has also been shown that the magnetic resonance of a periodic array of coupled silver strips with sub-wavelength periodicity is always accompanied by an electric anti-resonance; this is the periodicity effect and it does not occur for the case of an isolated strip pair of the same structural dimensions and materials. Recent studies [3,5,7] show that the destructive effect of the electric anti-resonance, which tends to make  $\varepsilon'$  (as well as  $n'$ ) positive, can be straightforwardly compensated by adding background metallic elements (non-resonant strips or wires, continuous or semi-continuous films), and that it is mostly the negative effective permeability that holds the key for advancing the design of low-loss NIMs in optics. Previously reported important results with different periodic metal-dielectric composites have already been obtained in the terahertz and subsequently in the infrared spectral ranges [7-11]. (Herein we are not considering a recent report on negative magnetism and negative refractive index in the green light range [12] because the subsequent careful studies performed by two independent groups show that both claims do not have grounds [13]).

This paper deals with the experimental observation of a negative permeability in the visible range in a periodic array of pairs of thin silver strips. For our study, two samples (denoted as Sample A and B) with slightly different geometries and different silver surface roughness have been fabricated. A negative effective permeability has been retrieved using numerical simulations; the results are in good agreement with the transmission and reflection spectra obtained from optical measurements for each sample. The value of  $\mu'$  is about  $-1$  in Sample A and about  $-1.7$  in Sample B at the wavelengths of 770 nm and 725 nm, respectively.

In addition to the predicted negative permeability and electric anti-resonances, abnormal enhanced absorption near the resonances due to imperfections in the fabricated NIM structures is also observed experimentally. Samples with different silver surface roughnesses

were fabricated by varying the silver deposition rate from 80 Å/s to 0.5 Å/s. Our results shown that a lower deposition rate provides lower roughness. The simulated absorbance was matched with the experimental absorbance by incorporating an adjusted value of the bulk-metal permittivity of silver,  $\varepsilon = \varepsilon' + i\alpha\varepsilon''$ , with a suitable wavelength dependent factor,  $\alpha$ . This deviation appears to be significant at the electric and magnetic resonances of the fabricated samples, while outside the resonances  $\alpha$  is close to 1. Since at the resonances the magnitude of the non-propagating modes is radically increasing, we conclude that these modes strongly interact with the inhomogeneities of the silver structures, resulting in the observed additional losses. Thus using the experimentally-matched losses in silver, we demonstrate a negative magnetic response from a periodic optical material for visible (red) light and discuss new challenges due to significantly increased losses that are observed at the resonances in actual “imperfect” thin silver strips. The roughness results in a decreased negative permeability relative to the ideal strips by factor 7.8 for Sample A and only by a factor 2.4 for Sample B, which has better surface quality.

Figure 1(a) shows the initial ideal elementary cell that we have used to optimize a negative permeability sub-wavelength grating. It consists of a pair of thin silver strips with thickness  $t$  and width  $w$ . The strips are separated by an alumina spacer with thickness  $d$ , width  $w$ , and a refractive index of  $n = 1.62 + 0i$ . The sub-wavelength lattice constant of the grating is  $p$ . The structure has been optimized using custom computer coding based on the spatial harmonic analysis (SHA) approach [14] with additional fabrication constraints pertinent to electron beam lithography. In the optimal structure, the periodicity  $p$  was chosen to be 300 nm with  $t = 35$  nm,  $d = 40$  nm, and  $w = 140$  nm, and isotropic bulk optical properties of silver have been taken from [15]. In the resonant (TM) polarization, the magnetic field is aligned with the largest dimension – the infinite length of the strips. Only one component of the magnetic field should ideally be present in this case. In the non-resonant (TE) polarization, the single component of the electric field is aligned with the strip length, giving no resonant effects. In such an ideal sub-wavelength grating of Fig. 1(a), a relatively wide negative magnetic response exists in the TM regime and extends from a wavelength of 720 nm to 825 nm, as shown in Fig. 1(b). A sharp electric resonant behavior is also demonstrated for the structure in TM mode around 500 nm. The electric resonance introduces a magnetic anti-resonance response within their common wavelength range. A reversed effect is observed at the magnetic resonance, where the electric anti-resonance is now present. The presence of anti-resonance makes it difficult to overlap the magnetic and electric resonances, since as the electric and magnetic resonances get closer to each other, the anti-resonances increase in

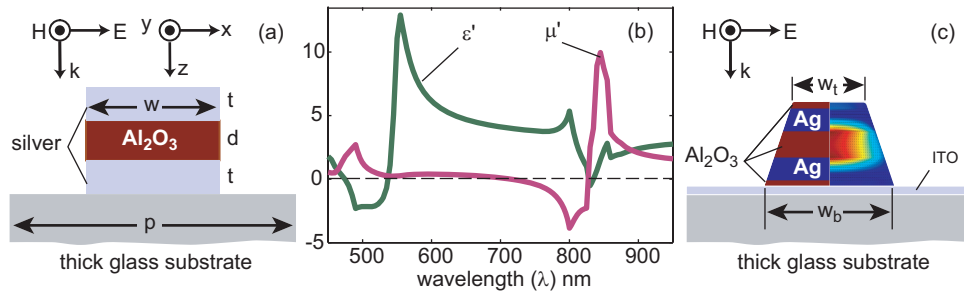


Fig. 1. (a). Ideal unit cell for the array of coupled silver nano-strips of width  $w$  that are separated by an alumina spacer of the same width; here  $t$  is the thickness of both strips and  $d$  is the thickness of the spacer. The strips are infinite in  $y$  and periodic in  $x$  with period  $p$ . (b) The real part of  $\varepsilon$  and  $\mu$  shown for the cell with  $w = 140$  nm,  $t = 35$  nm,  $d = 40$  nm, and  $p = 300$  nm. The optical constants of bulk silver [15] are taken for the strips. The refractive index of the substrate is 1.52. (c) The actual cross-section of samples obtained after fabrication (left half). Right half shows that the total B-field between the strips is opposite to the incident H-field at the magnetic resonance.

strength, resulting in the damping of the resonances [3].

Figure 1(c) shows a cross-section of the structure adjusted relative to the ideal structure of Fig. 1(a) in order to reflect fabrication realities. The fabrication procedure results in a trapezoidal shape of the stacked strips. Therefore, in contrast to the ideal structure, in the actual cross-section the top width  $w_t$  is smaller than the bottom width  $w_b$ . In addition, two thin 10-nm layers of alumina are added, one between the lower silver strip and the substrate and the second on top of the structure. The top alumina layer preserves the silver layer during the lift off process and makes the fabrication reproducible.

Electron beam lithography techniques have been used to fabricate the samples. First, the geometry of the periodic thin silver strips was defined by use of an electron beam writer on a glass substrate initially coated with a 15-nm film of indium-tin-oxide (ITO). Then, electron beam evaporation was applied to produce a stack of lamellar films. Finally, a lift-off process was performed to obtain the desired silver strips.

Measurements of the root-mean square (RMS) value of surface roughness using an atomic-force microscope (AFM) indicated that a slower deposition rate (0.5 Å/s, Sample B) of silver resulted in lower surface roughness than a faster deposition rate ( $\sim 2$  Å/s, Sample A). Note that the deposition rate cannot be set lower than 2 Å/s using a typical deposition procedure, since the deposition of silver heats of the resist material and makes the lift-off process impossible. To cool down the resist, we performed an original 4-step deposition process with 10-minute pauses between each deposition step. This new procedure allows the

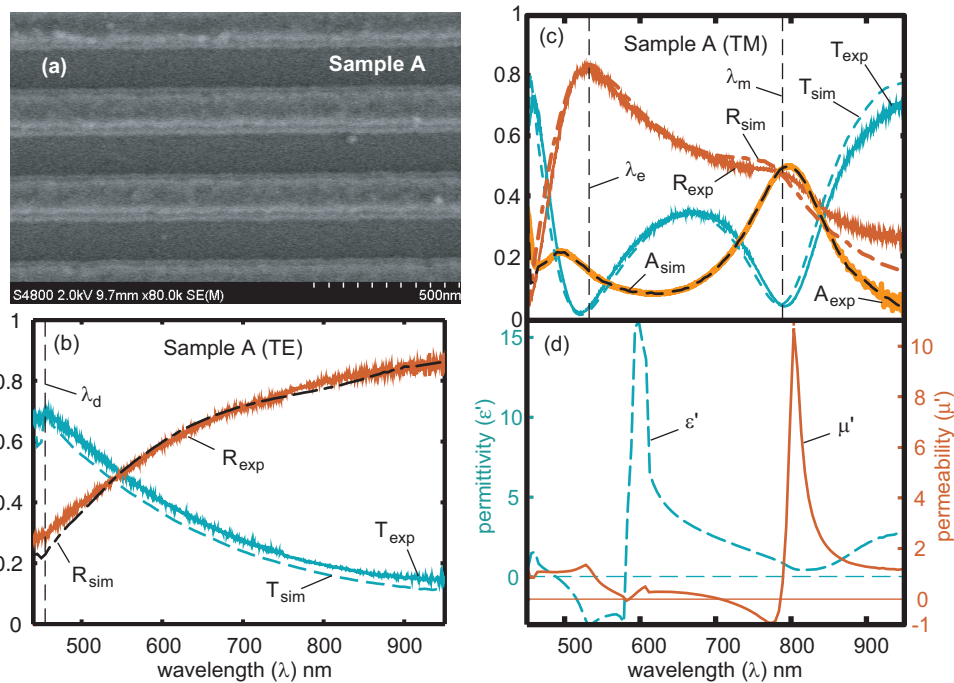


Fig. 2. (a) FE SEM picture of the periodic array of coupled silver strips (Sample A). (b) Transmission and reflection spectra of Sample A measured at normal incidence with TE polarization, here  $\lambda_d$  is the diffraction threshold. The experimental spectra are compared to the results of numerical modeling. The optical constants of silver strips are taken from the experimental data for bulk silver [15]. (c) Transmission, absorption and reflection spectra of Sample A at normal incidence with TM polarization compared to spectra obtained from simulations. In this case,  $\epsilon''$  of the silver strips was adjusted to match excessive losses. (d) The real part of the effective permeability ( $\mu'$ ) and effective permittivity ( $\epsilon'$ ).

use of a slower deposition rate of about 0.5 Å/s in order to obtain a lower surface roughness while ensuring successful lift-off, providing an overall better quality sample. The projected serial structure of the films from the ITO-coated glass was: Sample A, 10 nm alumina, 30 nm silver, 40 nm alumina, 30 nm silver, 10 nm alumina; Sample B, 10 nm alumina, 35 nm silver, 40 nm alumina, 35 nm silver, 10 nm alumina. A representative FE SEM image of the fabricated structure of Sample A is shown in Fig. 2(a), while Sample B is shown in Fig. 3(a).

To test the fabricated samples, we measured the transmission and reflection spectra of the samples with an ultra-stable tungsten lamp (B&W TEK BPS100). The spectral range of the lamp covers the entire visible and near-infrared optical band. A Glan Taylor prism was placed at the output of the broadband lamp to select light with desired linear polarization. The signal transmitted (or reflected) from the sample was introduced into a spectrograph (Acton SpectraPro 300i) and eventually collected by a liquid nitrogen cooled CCD-array detector. The transmission and reflection spectra were normalized to a bare substrate and a calibrated silver mirror, respectively. In the TE regime the electric field of the incident light was linearly polarized parallel to the length of silver strips, while in TM mode the electric field was rotated 90 degrees relative to TE case. For example, Figs. 2(b) and 2(c) show transmission and reflection spectra obtained from the optical measurements of Sample A for TE and TM polarizations at normal incidence.

In our simulations with a commercial finite element software package (more suitable for modeling the exact geometrical details of the structure than the SHA code), an incident plane wave source was placed at the source end of the computational domain, and the transmitted and reflected field amplitudes were monitored at two points located inside the domain several wavelengths away from the film under test.

The optical constants of silver used in the ideal model have been initially taken from experimental data [15] to obtain the optimal structure; as a result, a substantially negative  $\mu'$  has been obtained as shown in Fig. 1(c). In the ideal situation, both the experimental and simulation setup would allow for an adequate match of the reflection and transmission spectra of light in both polarizations. The transmission spectrum with TE polarization is shown in Fig. 2(b). In this case, as expected, both spectra match well over a broad range of measured wavelengths. The measured spectra display a moderate non-resonant wavelength dependence and low, almost constant, absorption; transmission falls off closer to the higher wavelengths. The relaxed wavelength dependence is attributed to non-resonant behavior of the metallic strips diluted with the alumina spacer in a layer that could be adequately described by the effective medium theory. Good matching occurs almost everywhere, provided that the light in the measured and simulated structures has a single propagating mode (no diffraction). Beyond 950 nm the signal-to-noise ratio worsens, making signal detection difficult at the output.

A useful feature of the optical TE measurements is that the spectral position of the diffraction threshold, shown in Fig. 2(b) as  $\lambda_d$ , is a direct indicator of the true effective periodicity observed in the experiment. Indeed, as long as the refractive index of the substrate,  $n_s$ , is known almost exactly, a simple and accurate measurement of the actual period can be obtained from  $p = \lambda_d/n_s$ . Similar to the TE mode, the TM polarization gives useful data for measuring the actual geometry of the samples obtained after fabrication. Specifically, the spectral position of the electric and magnetic resonances  $\lambda_e$  and  $\lambda_m$  shown in Fig. 2(c) are both very sensitive to the thickness and width of the metallic strips. Good agreement with the experimental spectra of Figs. 2(c) and 2(b) has been achieved by varying these parameters within realistic fabrication tolerances. Thus, the silver strips used in the simulation of Sample A were 4 nm thinner and 8 nm wider than initial estimates from FE SEM images. Additional examinations of FE SEM images taken in a number of areas over the sample are consistent with this result. As expected, spectroscopic measurements appeared to be more accurate for the dimensions that are critical in the resonant regimes, giving a better result than estimates based on FE SEM images. In addition, clear-cut optical measurements of transmission and reflection spectra with both polarizations incorporate and level out imperfections inevitable in the fabrication process. It is also important to note that the deviations from the initially

planned thickness agree well with roughness estimates taken at the strip surface. Thus, in Sample A, where the surface roughness is within 2 – 6 nm, the actual thickness of the strips obtained by matching numerical simulations to spectroscopic measurements is about 26 nm versus a 30-nm thickness planned for this design. In accord with this, the strips of Sample B fabricated with a lower deposition rate and demonstrating much lower roughness (about 1.5 – 2.5 nm) do not show any discernable deviation from the planned thickness of 35 nm. The dimensions of the samples taken in the simulations are: Sample A,  $t = 26$  nm,  $d = 48$  nm,  $w_t = 94$  nm, and  $w_b = 174$  nm; Sample B,  $t = 35$  nm,  $d = 40$  nm,  $w_t = 85$  nm, and  $w_b = 160$  nm.

In contrast to the TE case, where the optical constants of the bulk silver are used to describe the optical behavior of silver strips, the TM polarization reveals substantial discrepancies in the optical properties (specifically, in absorption) of the nano-structured silver strips in comparison to the data shown for ideal strips with the permittivity of bulk silver in Ref. [15]. Specifically, the experimental absorption is larger than that obtained through simulations. This enhanced absorption is due to the roughness features and other imperfections in the fabricated structures. We model the contributions from these imperfections through a wavelength-dependent adjustment factor  $\alpha$  such that the permittivity of silver is given by  $\epsilon = \epsilon' + i\alpha\epsilon''$ . The computed results of the transmission, absorption and reflection spectra using the adjusted (imaginary part of) permittivity of bulk silver are shown in Figs. 2(c) and 3(c). The employed adjustment factor  $\alpha$  is shown in Fig. 3(b).

In both samples at the TM polarization the loss adjustment is significant for the electric resonance and especially large for the magnetic resonance. Away from the electric and magnetic resonances at both polarizations, the presence of small roughness features on the metal strips has a very small effect such that almost no adjustment to  $\epsilon''$  is needed. As shown

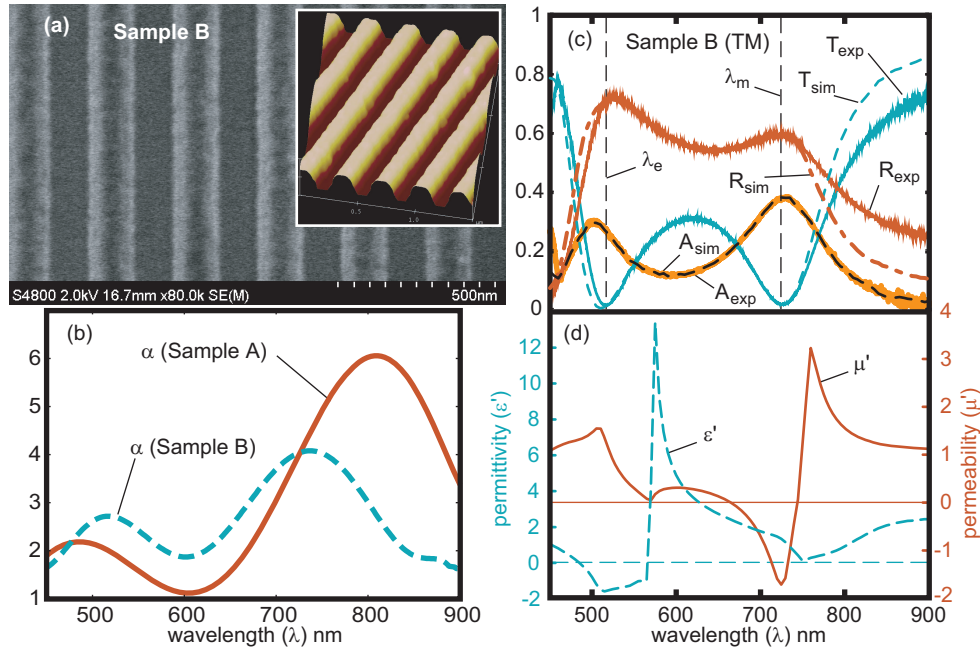


Fig. 3. (a) FE SEM picture of Sample B. (The inset shows an AFM image of the sample.) (b) Comparison of the loss-adjustment factor  $\alpha$  obtained for Samples A and B. Sample A demonstrates more excessive loss in comparison to bulk metal [15] and Sample B. (c) Transmission, absorption and reflection spectra of Sample B at normal incidence with TM polarization compared to spectra obtained from simulations. In this case,  $\epsilon''$  of the silver strips was adjusted to match excessive losses. (d) The real part of the effective permeability ( $\mu'$ ) and effective permittivity ( $\epsilon'$ ). A minimum  $\mu'$  of  $-1.7$  is obtained at 725 nm.

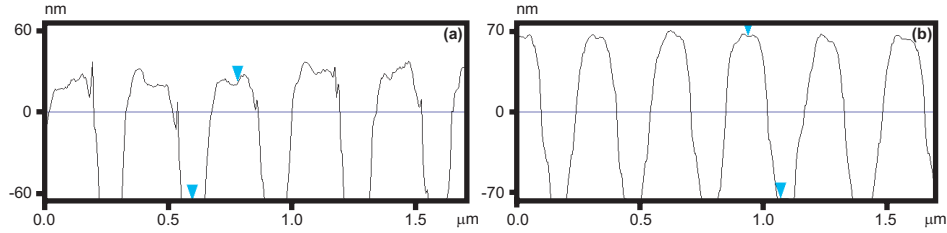


Fig. 4. Section analysis obtained from AFM scans of Sample A and Sample B (shown in panels (a) and (b) respectively).

in Fig. 3(b), the adjustment factor  $\alpha$  is almost one between the resonances in Sample A. In Sample B, the resonances are closer and overlap more, requiring a slightly larger adjustment between the resonances. Concurrently at the magnetic resonance, the lower surface roughness of the strips in Sample B requires a lower adjustment ( $\max(\alpha) \approx 4$ ) than for Sample A ( $\max(\alpha) \approx 6$ ).

The above results are consistent with the statistical analysis of surface roughness obtained from AFM scans. Example cross sections of the AFM images, shown in Fig. 4(a) for Sample A and in Fig. 4(b) for Sample B, indicate a substantial difference in the surface roughness of the samples. To extract quantitative characteristics a root mean square (RMS) roughness analysis was performed using seven  $60 \times 60 \text{ nm}^2$  areas. For each sample the areas were selected from the tops of randomly chosen strips. The Sample A roughness is characterized by larger variations in the RMS between seven areas ranging from 2 to 6 nm (versus 1.5 – 2.5 nm variations for Sample B) with the value of the RMS over the total area being about 3.7 nm (versus 2 nm for Sample B).

A similar correction for  $\varepsilon''$  of silver in an optical metamaterial has been recently implemented by using a wavelength-independent factor ( $\alpha = 3$ ) [6,16]. Figure 5 illustrates this approach, where  $\alpha = 3$  is also used. Figure 5(a) shows that the constant  $\alpha$  demonstrates somewhat better conformity with the T and R spectra than shown in Ref. [16] for a more complex structure, but still worse than the agreement achieved in Fig. 3(c) using the wavelength-dependent factor of Fig. 3(b). In addition the underestimated losses tend to make  $\mu'$  artificially more negative, as shown in Figs. 5(a) and 5(b).

The ideal spectra of  $\mu'$  computed for “ideal prototypes” without any adjustment to the permittivity of bulk silver have also been compared with the values of  $\mu'$  calculated with the

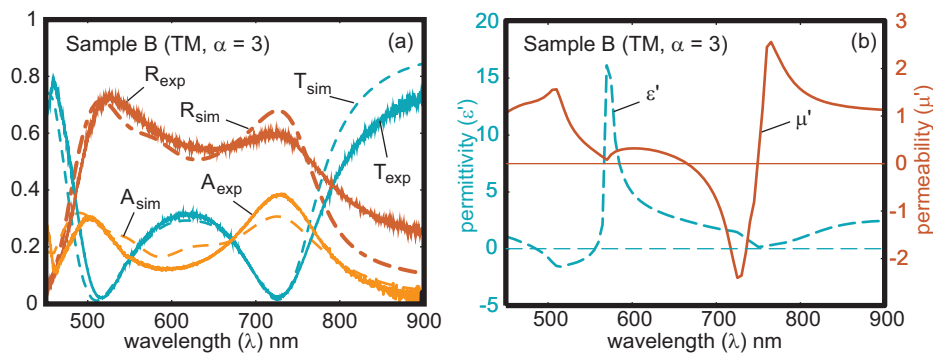


Fig. 5. (a). Transmission, absorption and reflection spectra of Sample B at normal incidence with TM polarization compared to spectra obtained from simulations; here  $\varepsilon''$  of silver was adjusted using a factor of  $\alpha = 3$ . (b) The real part of the effective values of  $\mu'$  and  $\varepsilon'$  obtained using the wavelength-independent factor  $\alpha = 3$ .

adjustment factor of Fig. 3(b). The “ideal prototypes” have the same dimensions, including trapezoidal shaped cross-sections, as those of the experimental Samples A and B, but the “ideal prototypes” are simulated with no loss adjustment ( $\alpha = 1$ ). Relative to the “ideal prototypes” with an ideal metal surface, negative magnetism is reduced by a factor of 7.8 in Sample A and only by a factor of 2.4 in Sample B. Most importantly, this comparison clearly indicates that by fabricating strips with minimized roughness features, the magnetic response of the metamaterial can be dramatically increased.

In summary, we have designed, fabricated and measured two samples with negative permeabilities of  $-1$  and  $-1.7$  at 770 nm and 725 nm, respectively. Detailed numerical models of the samples have been used to validate the measurements, where an adjusted wavelength-dependent  $\epsilon''$  is used in silver at the resonances to model the effect of surface roughness. The results of the numerical modeling are compared with the experimental data. The good agreement between experiment and theory achieved for two different polarizations in a wide wavelength range is excellent proof of the validity of the model, hence confirming the existence of negative permeability at red light. We also discuss the difficulties in automated optimization of NIMs due to substantial deviations from the ideal, smooth silver strip surface. These deviations result in enhanced absorption at the resonances which were observed experimentally in the resonant plasmonic elements of our nano-structured samples. These non-idealities would require constant feedback from fabrication and measurements in order to optimize low-loss NIMs in visible range. The results also indicate that by further improving the fabrication methods to minimize the imperfections causing the increased losses, one can obtain a much stronger negative magnetic response.

#### **Acknowledgments**

The authors are grateful to Prof. Minghao Qi and Maroof Khan for their help with fabrication. This work was supported in part by ARO grant W911NF-04-1-0350, NSF-PREM Grant #DMR-0611430 and by ARO-MURI award 50342-PH-MUR.